A Modified Hopfield Neural Network for Perfect Calculation of Magnetic Resonance Spectroscopy

HAZEM M. EL-BAKRY

Faculty of Computer Science & Information Systems,
Mansoura University, EGYPT
helbakry20@yahoo.com

NIKOS MASTORAKIS

Dept. of Computer Science
Military Institutions of University Education
(MIUE) - Hellenic Academy, Greece

***Abstract*—** In this paper, an automatic determination algorithm for nuclear magnetic resonance (NMR) spectra of the metabolites in the living body by magnetic resonance spectroscopy (MRS) without human intervention or complicated calculations is presented. In such method, the problem of NMR spectrum determination is transformed into the determination of the parameters of a mathematical model of the NMR signal. To calculate these parameters efficiently, a new model called modified Hopfield neural network is designed. The main achievement of this paper over the work in literature [30] is that the speed of the modified Hopfield neural network is accelerated. This is done by applying cross correlation in the frequency domain between the input values and the input weights. The modified Hopfield neural network can accomplish complex dignals perfectly with out any additinal computation steps. This is a valuable advantage as NMR signals are complex-valued. In addition, a technique called "modified sequential extension of section (MSES)" that takes into account the damping rate of the NMR signal is developed to be faster than that presented in [30]. Simulation results show that the calculation precision of the spectrum improves when MSES is used along with the neural network. Furthermore, MSES is found to reduce the local minimum problem in Hopfield neural networks. Moreover, the performance of the proposed method is evaluated and there is no effect on the performance of calculations when using the modified Hopfield neural networks.

***Keywords*—** Hopfield Neural Networks, Cross Correlation, Nuclear Magnetic Resonance, Magnetic Resonance Spectroscopy, Fast Fourier Transform.

I. Introduction

Applications of magnetic resonance imaging were started in magnetic resonance imaging (MRI) which is a technique imaging the human anatomy, and they include various specialized technique such as diffusion-weighted imaging (DWI), perfusion-weighted imaging (PWI), magnetic resonance angiography (MRA) and magnetic resonance cholangio-pancreatography (MRCP). Functional MRI (fMRI) that is an innovative tool for functional measurement of human brain and that is a technique imaging brain functions, also became practical and has been widely used in recent years. In contrast with MRI and fMRI, magnetic resonance spectroscopy (MRS) is a technique that measures the spectra of the metabolites in a single region, and magnetic resonance spectroscopic imaging (MRSI), which obtains the spectra from many regions by applying imaging techniques to MRS, has also been developed. Although 31P-MRS was widely performed in MRS before, proton MRS is primarily performed recently. 13C-MRS using heteronuclear single-quantum coherence (HSQC) method has also been developed recently. MRS and MRSI, however, have remained underutilized together due to their technical complexities compared with MRI.

At present, MRS is technically evolved and its operation has remarkably improved. The measurement of MRS also has started to be automatically analyzed and indicated, and there are some representative analysis software introduced in the Internet, LCModel: an automatic software packages for in-vivo proton MR spectra including the curve-fitting procedure [41], and MRUI: Magnetic Resonance User Interface including the time-domain analysis of in-vivo MR data [31,44]. The technique proposed in this paper is also used for in the time-domain. It probably a better result of the analysis is obtained by combining the algorithms of MRUI with our technique, because both of them are performed in the time-domain.

MRSI has the big feature that is not in MRI and fMRI, that is, it can detect internal metabolite non-invasively, track the metabolic process and perform the imaging. Thus the importance of it is huge. Furthermore, MRSI is also expected as an imaging technique realizing the molecular imaging. I believe that MRSI has the value beyond fMRI, because of its potential.

For commonly performing the MRSI, it is an indispensable technique to quantify NMR spectra automatically, and it is also expected to progress the automatic analysis techniques. Therefore, it is necessary to develop a novel method introducing neural network techniques including our proposing method, as well as existing analysis software. Consequently, it is important to proceed with the research of this territory.

MRS is used to determine the quantity of metabolites, such as creatine phosphate (PCr) and adenocine triphosphate (ATP), in the living body by collecting their nuclear magnetic resonance (NMR) spectra. In the field of MRS, the frequency spectrum of metabolites is usually obtained by applying the algorithm of fast Fourier transform (FFT [4]) to the NMR signal obtained from the living body. Then, quantification of the metabolites is carried out by estimating the area under each

spectral peak using a curve fitting procedure [25,29,45]. However, this method is not suitable for processing large quantities of data because human intervention is necessary. The purpose of this paper is to present an efficient automatic spectral determination method to process large quantities of data without human intervention.

This paper is organized as follows: in section II, Conventional determination methods of NMR spectra are described and a brief outlines of the proposed algorithm is given. An over efficient view of NMR signal theory; a mathematical model of the NMR signal are discussed. The proposed approach to spectral determination is presented. Design of complex-valued Hopfield neural networks for fast and efficient spectral estimation is introduced in section III. MODIFIED SEQUENTIAL EXTENSION OF SECTION (MSES) explains the concept of MSES. For performance evaluation of the proposed method, simulations were carried out using sample signals that imitate an actual NMR signal, and the results of those simulations are given. The results are evaluated and discussed in Section IV. Finally, conclusions and future work are given.

II. Mathematical Model of the NMR Signal and Determination of Spectra

Magnetic resonance imaging (MRI) systems, which produce medical images using the nuclear magnetic resonance (NMR) phenomenon, have recently become popular. Additional technological innovations, such as high-speed imaging technologies [10,15,26,27,28] and imaging of brain function using functional MRI [2,24,40] are also rapidly progressing. Currently, the above-mentioned imaging technologies mainly take advantage of the NMR phenomena of protons. The atomic nuclei used for analyzing metabolism in the living body include proton, phosphorus-31, carbon-13, fluorine-19 and sodium-22. Phosphorus-31 NMR spectroscopy has been widely used for measurement of the living body, because it is able to track the metabolism of energy.

NMR was originally developed and used in the field of analytical chemistry. In that field, NMR spectra are used to analyze the chemical structure of various materials. This is called NMR spectroscopy. In medical imaging, it is also possible to obtain NMR spectra. In this case, the technique is called magnetic resonance spectroscopy (MRS), and it can be used to collect the spectra of metabolites in organs such as the brain, heart, lung and muscle. The difference between NMR spectroscopy and MRS is that in MRS, spectra is collected from the living body in a relatively low magnetic field (usually, about 1.5 Tesla); in NMR spectroscopy, small chemical samples are measured in a high magnetic field.

In MRI systems, Fourier transform is widely used as a standard tool to produce an image from the measured data and to obtain NMR spectra. In NMR spectroscopy, a frequency spectrum can be obtained by applying the fast Fourier transform (FFT) to the free induction decay (FID) that is observed as a result of the magnetic relaxation phenomenon [7]. Here the FID is an NMR signal in the time domain and it is a time series, that is, it can be modeled as a set of sinusoids exponentially damping with time. When FFT is applied to such a signal, the spectral peaks obtained are of the form called a Lorentz curve [7]. If the signal is damped rapidly, the height of the spectral peaks will be decreased and the width of the peaks will increase. This is an inevitable result of applying FFT to FIDs. In addition, the resolution of the spectrum collected in a low magnetic field is much lower than a typical spectrum obtained by NMR spectroscopy. Therefore, the problems of spectral analysis in MRS and NMR spectroscopy are quite different. The spectral peaks obtained in MRS are spread out and the spectral distribution obtained is very different from the original distribution. Therefore, peak height to quantify metabolites cannot be used. Instead, the area under each peak is estimated by using curve-fitting procedures (non-linear least square methods) [25,29,45]. However, existing curve-fitting procedures are inadequate for processing large quantities of data because they require human intervention. The aim of our research is to devise a method that does not require such human intervention.

Two approaches can be considered to solve this problem: (1) automating the description of spectral peaks and the determination of the peak areas, and (2) using methods of determination and quantification other than the Fourier transform. In the first approach, attempts at automatic quantification of NMR spectra using hierarchical neural networks have been reported [1,22]. In this research, a three-layered network based on back propagation [42] was employed and the spectra in the frequency domain were used as the training data of the network. The fully-trained network had the ability to quantify unknown spectra automatically, and curve fitting procedures were not necessary. However, large amounts of training data were necessary to increase the precision of quantification. These methods quantify the spectra instead of performing the curve fitting procedures. In the second approach, the maximum entropy method (MEM), derived from the autoregressive (AR) model and the linear prediction (LP) method, and other similar methods have been studied widely [14,44]. These are parametric methods, that is, in these methods, a mathematical model of the signal is assumed and the parameters of that model are estimated from observed data. The spectrum can then be estimated from the model parameters. However, methods based on AR modeling require large amounts of calculation.

The main objective of this research is to develop a method to estimate NMR spectra without human intervention or complicated calculations. Therefore, a parametric approach, in which a neural network is used [13], is considered. Fixed weights Hopfield neural networks [82,84] are used. It is possible to estimate the parameters using the ability of these neural networks to find a local minimum solution or a minimum solution. In addition, it was noted that NMR signals are complex-valued and a method to estimate the spectrum using complex-valued Hopfield networks [18,46], in which the weights and thresholds of conventional networks are expanded to accommodate complex numbers, was developed. Both a hierarchical type [3,12,32] and a recurrent type [21] have been proposed. The operation of these networks was accelerated as described by [8,9] and this is main achievement of this paper. Furthermore, a technique that takes into account the damping

of the NMR signal, which we call "sequential extension of section" (MSES) has been devised, and used with the above-mentioned network.

a) Mathematical model of NMR signal

If an atomic nucleus possessing a spin is placed in a static magnetic field, it begins a rotation called "precession" around the direction of the static magnetic field. It is assumed that the direction of the static magnetic field is the z-direction, and the orthogonal plane for the z-direction is the x-y plane. Considering an atomic ensemble, a macroscopic magnetization M resulting from the sum of the spin of each nucleus appears in the z-direction. When the ensemble is exposed to an external rotating magnetic field at the resonance frequency of the precession, each nucleus in the ensemble resonates. As a result, a component of magnetization in the x-y plane appears, and the component in the z-direction decreases. It is assumed that the magnetization M has rotated and is now operating around the z-axis. The resonant magnetic field pulse that tilts M 90 degrees to the x-y plane is called a 90-degree pulse.

After a 90-degree pulse, the magnetization M returns to its original orientation in the z-direction. During that time, the component in the x-y plane is exponentially damped with time t and time constant T_2, so the signal is represented by an equation in the form $\exp(-t/T_2)$. The component in the z-direction recovers with time t and time constant T_1; this process is represented by an equation in the form $1-\exp(-t/T_1)$. This phenomenon is called the magnetic relaxation. The change in the component in the x-y plane is called the transverse relaxation, and the change in the component in the z-direction is called the longitudinal relaxation. T_2 and T_1 are called the transverse relaxation time and the longitudinal relaxation time, respectively. Because of inhomogeneity in the static magnetic field, the transverse relaxation time is actually shortened. Thus, we usually observe this shortened transverse relaxation, called T_2^* ($T_2^* < T_2$), unless we use a technique such as the spin echo method [7].

In NMR, the component in the x-y plane is called an "NMR signal" or "free-induction decay" (FID), and it is expressed in a complex form because it is in essence a rotation.

An NMR signal (FID) with *m* components is modeled as follows:

$$\hat{x}_n = \sum_{k=1}^{m} A_k \exp(-b_k n)\exp[j(2\pi f_k n+\phi_k)], \quad n=0,1,\cdots,N-1 \tag{1}$$

where $\hat{x}_n$ $(n=0,1,\cdots,N-1)$ denotes the observed signal, which is complex-valued, and n denotes the sample point on the time axis. $A_k, b_k, f_k,$ and ϕ_k denote the spectral composition, damping factor, rotation frequency, and phase in the rotation, respectively, of each metabolite, and m is the number of the metabolites composing a spectrum (each of these is a real number, and $j=\sqrt{-1}$).

b) NMR spectra

The position of each peak appearing in a NMR spectrum depends on its offset frequencies (chemical shifts) from the resonance frequency of a target nucleus under a specified static magnetic field [7]. These offset frequencies are f_k (k=1,…,m).

In a common pulse method, each peak possesses the offset phase expressed by a linear function of its offset frequencies f, as follows [7]:

$$\theta(f) = \alpha + \beta \cdot f \tag{2}$$

where, α is called the zero-dimensional term of phase correction, and is a common phase error influencing each peak. β is called the one-dimensional term of phase correction, and is a phase error that is dependent on the offset frequencies, or more specifically, the positions of each peak.

Thus, in NMR spectra, the position of each peak and the scale of their offset phase are decided by the measurement condition used. Because of this fact, it is possible to make a rough prediction of the position of each peak of a NMR spectrum under specified measurement conditions. This positional can be used as a constrained condition when estimating unknown parameters using neural networks. In addition, because the relationship between a specified static magnetic field and the apparent transverse relaxation time T_2^* of a target nucleus are known in MRS [14], it is possible to determine the rough scale of T_2^* for a target nucleus when the strength of the static magnetic field is known. This information regarding T_2^* can also be used as a constrained condition. That is, it can be used for the determination of b_k.

c) Determination of NMR spectra

The following approach is used in our method of parametric spectral determination.

(1) A mathematical model of the NMR signal is given, as described above.
(2) Adequate values are supplied as initial values of the parameters $A_k, b_k, f_k,$ and ϕ_k, and an NMR signal is simulated.
(3) The sum of the squares of the difference, at each sample point, between the simulated signal and the actual observed signal is calculated.
(4) The parameters are changed to give optimum estimates for the observed signal by minimizing the sum-squared error.

III. Design of Modified Hopfield Neural Network for Spectral Estimation

Conventional Hopfield neural networks accept input signal with fixed size (n). Therefore, the number of neurons equals to (n). Instead of treating (n) inputs, the idea is to collect all the input data together in a long signal (for example 100xn). Then the input signal is processed by Hopfield neural networks as a single pattern with length L (L=100xn). Such a process is performed in the frequency domain.

Given any two functions f and d, their cross correlation can be obtained by:

$$d(x)\otimes f(x)=\left(\sum_{n=-\infty}^{\infty} f(x+n)d(n)\right) \quad (3)$$

Therefore, the output of each neuron can be written as follows [8,9]:

$$O_i = g\left(W_i \otimes Z\right) \quad (4)$$

where Z is the long input signal, W is the weight matrix, O_i is the output of each neuron and g is the activation function.

Now, the above cross correlation can be expressed in terms of one dimensional Fast Fourier Transform as follows:

$$W_i \otimes Z = F^{-1}\left(F(Z)\bullet F^{*}\left(W_i\right)\right) \quad (5)$$

It is clear that the operation of the modified Hopfield neural network depends on computing the Fast Fourier Transform for both the input and weight matrices and obtaining the resulting two matrices. After performing dot multiplication for the resulting two matrices in the frequency domain, the Inverse Fast Fourier Transform is calculated for the final matrix. Here, there is an excellent advantage with the modified Hopfield neural network that should be mentioned. The Fast Fourier Transform is already dealing with complex numbers, so there is no change in the number of computation steps required for the modified Hopfield neural network. Hence, by evaluating this cross correlation, a speed up ratio can be obtained comparable to conventional Hopfield neural networks.

For the determination of NMR spectra, the sum-squared error of the parameter determination problem is defined as the energy function of a Hopfield network. This converts the parameter determination problem to an optimization problem for the Hopfield network. The energy function is defined as:

$$E=-\frac{1}{2}\sum_{n=0}^{N-1}\left|\hat{x}_n - \sum_{k=1}^{m} A_k \exp(-b_k n)\exp\{j(2\pi f_k n + \phi_k)\}\right|^2 \quad (6)$$

where, as in Eq.(1), n denotes the sample point on the time axis and $\hat{x}_n$ denotes the complex-valued observed signal at n.

The energy function E of complex-valued neural networks should have the following properties [23]:

(1) A function that relates the state $\hat{x}$ denoted by a complex number to a real-valued number.

(2) To converge on the optimum solution, it is always necessary to satisfy the following condition in the dynamic updating of the Hopfield network:

$$\frac{dE(\cdot)}{dt} \le 0 \quad (7)$$

The energy function defined by Eq.(6) satisfies property 1. In Eq.(6), if

$$\hat{d}_n = \hat{x}_n - \sum_{k=1}^{m} A_k \exp(-b_k n)\exp\{j(2\pi f_k n + \phi_k)\}, \quad (8)$$

then the energy function can be expressed as:

$$E=-\frac{1}{2}\sum_{n=0}^{N-1}\left|\hat{d}_n\right|^2=-\frac{1}{2}\sum_{n=0}^{N-1}\hat{d}_n\hat{d}_n^{\,*} \quad (9)$$

(*: denotes the complex conjugate)

From Eq.(6), when the parameters A_k, b_k, f_k, and ϕ_k in Eq.(1) are replaced by P_k, the time variation of the above energy function can be expressed as

$$\frac{dE}{dt}=\sum_{k=1}^{m}\sum_{P_k}\frac{\partial E}{\partial P_k}\frac{dP_k}{dt},(P_k; A_k, b_k, f_k, \phi_k, k=1,\cdots,m) \quad (10)$$

Here, suppose that

$$\frac{dP_k}{dt}=-\left(\frac{\partial E}{\partial P_k}\right)^{*} \quad (11)$$

Then,

$$\frac{dE}{dt} = -\sum_{k=1}^{m}\sum_{P_k}\left|\frac{\partial E}{\partial P_k}\right|^2 \le 0 \quad (12)$$

will hold, and property 2 is satisfied, so convergence in the dynamic updating of the modified complex-valued Hopfield neural network is guaranteed.

From Eq.(9), the variation of the energy function with the variation of the parameters is as follows:

$$\frac{\partial E}{\partial P_k} = -\frac{1}{2}\sum_{n=0}^{N-1}\left(\frac{\partial \hat{d}_n}{\partial P_k}\hat{d}_n^{\,*} + \frac{\partial \hat{d}_n^{\,*}}{\partial P_k}\hat{d}_n\right) \quad (13)$$

From the form of the right-hand side of Eq.(13),

$$\left(\frac{\partial E}{\partial P_k}\right)^{*} = \frac{\partial E}{\partial P_k} \quad (14)$$

Then, by Eqs.(11) and (14), we have

$$\frac{dP_k}{dt} = -\frac{\partial E}{\partial P_k} = \frac{1}{2}\sum_{n=0}^{N-1}\left(\frac{\partial \hat{d}_n}{\partial P_k}\hat{d}_n^{\,*} + \frac{\partial \hat{d}_n^{\,*}}{\partial P_k}\hat{d}_n\right) \quad (15)$$

Equation (15) expresses the time variation of the parameters P_k, that is, the updating of the parameters. Suppose that $\hat{d}_n^{*}$ and $\hat{d}_n$ on the right-hand side of the equation are the inputs to the modified Hopfield neural network and $\partial\hat{d}_n/\partial P_k$ and $\partial\hat{d}_n^{*}/\partial P_k$ are the input weights in the network, then a Hopfield complex-valued network can be designed. The inputs and the input weights are then calculated by Eq.(8). In this network, two complex-valued input systems conjugated to each other are input to the network. The updating of the parameters is then carried out by

complex calculation. However, because the two terms on the right-hand side of Eq.(15) are complex conjugates of each other, the left-hand side is a real number. The structure of the complex-valued network is depicted in Fig.1, where the coefficient 1/2 in Eq.(15) is omitted. Two complex-valued input systems conjugated to each other are input to one unit, and the updating of the parameters is carried out by complex-valued calculation.

Eq.(8) can be decomposed into a real part $d_{re}(n)$ and an imaginary part $d_{im}(n)$:

$$\hat{d}_n = d_{re}(n) + jd_{im}(n) \tag{16}$$

Suppose that the real and imaginary parts of $\hat{x}_n$ are denoted as $x_r(n)$ and $x_i(n)$, respectively. Then we have:

$$d_{re}(n) = x_{re}(n) - \sum_{k=1}^{m} A_k \exp(-b_k n)\cos\{j(2\pi f_k n + \phi_k)\} \tag{17}$$

$$d_{im}(n) = x_{im}(n) - \sum_{k=1}^{m} A_k \exp(-b_k n)\sin\{j(2\pi f_k n + \phi_k)\} \tag{18}$$

From these,

$$\begin{aligned}\left|\hat{d}_n\right|^2 &= \hat{d}_n \hat{d}_n^* \qquad (*: \text{complex conjugate}) \\ &= \{d_{re}(n) + jd_{im}(n)\}\{d_{re}(n) - jd_{im}(n)\} \\ &= \left|d_{re}(n)\right|^2 + \left|d_{im}(n)\right|^2\end{aligned} \tag{19}$$

Then, Eq.(9) can be developed as follows:

$$E = -\frac{1}{2}\sum_{n=0}^{N-1}\left|\hat{d}_n\right|^2 = E_{re} + E_{im} \tag{20}$$

$$E_{re} = -\frac{1}{2}\sum_{n=0}^{N-1}\left|d_{re}(n)\right|^2 \tag{21}$$

$$E_{im} = -\frac{1}{2}\sum_{n=0}^{N-1}\left|d_{im}(n)\right|^2 \tag{22}$$

From Eqs.(10) and (20), we obtain

$$\begin{aligned}\frac{dE}{dt} &= \sum_{k=1}^{m}\sum_{P_k}\frac{\partial E}{\partial P_k}\frac{dP_k}{dt} \\ &= \frac{dE_{re}}{dt} + \frac{dE_{im}}{dt} \\ &= \sum_{k=1}^{m}\sum_{P_k}\left(\frac{\partial E_{re}}{\partial P_k} + \frac{\partial E_{im}}{\partial P_k}\right)\frac{dP_k}{dt}\end{aligned} \tag{23}$$

where,

$$\frac{dE_{re}}{dt} = \sum_{k=1}^{m}\frac{\partial E_{re}}{\partial P_k}\frac{dP_k}{dt} \tag{24}$$

$$\frac{dE_{im}}{dt} = \sum_{k=1}^{m}\frac{\partial E_{im}}{\partial P_k}\frac{dP_k}{dt} \tag{25}$$

$$(P_k;\ A_k,\ b_k,\ f_k,\ \phi_k)$$

Assume that

$$\frac{dP_k}{dt} = -\left(\frac{\partial E_{re}}{\partial P_k} + \frac{\partial E_{im}}{\partial P_k}\right) \tag{26}$$

$$(P_k;\ A_k,\ b_k,\ f_k,\ \phi_k,\quad k = 1,\cdots,m)$$

We can get the following:

$$\frac{dE}{dt} = \sum_{k=1}^{m}\sum_{P_k}\left|\frac{\partial E_{re}}{\partial P_k} + \frac{\partial E_{im}}{\partial P_k}\right|^2 \le 0 \tag{27}$$

From Eqs.(21) and (22), we obtain

$$\frac{\partial E_{re}}{\partial P_k} = -\sum_{n=0}^{N-1}\frac{\partial d_{re}(n)}{\partial P_k}d_{re}(n) \tag{28}$$

$$\frac{\partial E_{im}}{\partial P_k} = -\sum_{n=0}^{N-1}\frac{\partial d_{im}(n)}{\partial P_k}d_{im}(n) \tag{29}$$

Hence, Eq.(26) can be expressed as follows:

$$\begin{aligned}\frac{dP_k}{dt} &= -\left(\frac{\partial E_{re}}{\partial P_k} + \frac{\partial E_{im}}{\partial P_k}\right) \\ &= \sum_{n=0}^{N-1}\left(\frac{\partial d_{re}(n)}{\partial P_k}d_{re}(n) + \frac{\partial d_{im}(n)}{\partial P_k}d_{im}(n)\right) \\ &(P_k;\ A_k,\ b_k,\ f_k,\ \phi_k,\quad k = 1,\cdots,m)\end{aligned} \tag{30}$$

From Eqs.(15) and (30), the complex-valued network can be expressed as an equivalent real-valued network which has two real-valued input systems. That is, let the parameters change with time as shown in Eq.(30). Then, the energy function E satisfies property 2, above. Thus, convergence in the updating of the complex-valued network can be guaranteed. The equivalent network is depicted in Fig.2. The parameters are updated by the steepest descent method as follows:

$$\begin{aligned}P_k &= P_k + \varepsilon\frac{dP_k}{dt}, \qquad (\varepsilon > 0) \\ &(P_k;\ A_k,\ b_k,\ f_k,\ \phi_k,\quad k = 1,\cdots,m)\end{aligned} \tag{31}$$

For every parameter P_k, this equivalent network forms a unit which has two input systems, corresponding to the real and imaginary parts of the NMR signal. Each input system has an input d and an input weight $\partial \hat{d}_n / \partial P_k$ corresponding to the number of sample points. d is calculated by Eqs.(17) and (18), which means that the inputs and input weights are calculated using the previous values of the parameters and the observed signal. By means of this input, the state of the unit is changed and each parameter is updated. The input and the input weights are recalculated with the updated parameters. This is the equivalent network implemented in this paper.

Incidentally, k in Eqs.(30) and (31) represents one of the components of an NMR signal. Because Eq.(30) is applied to each k, the updating of parameters A_k, b_k, f_k, and ϕ_k is simultaneously carried out on k. As described, in the network used in this paper, the sequential updating of each unit, which is a feature of the Hopfield network, is transformed to sequential updating of every unit group A_k, b_k, f_k, and ϕ_k on k.

As expressed in Eq.(1), the NMR signal is a set of sinusoidal waves in which the spectral components A_k are exponentially damped with time n. The operation shown in Fig. 3 is introduced so that the proposed network would recognize the decay state more accurately. In the figure, the horizontal axis shows the sample points at time n, and the vertical axis shows the NMR signal. In this operation, first, appropriate values are assigned as initial values for each of the parameters. Then, our network operates on section A from time 0 ($n = 0$) to an adequate time k_1 ($n = k_1$). The parameter estimates are obtained when the network has equilibrated. Next, the network operates on section B from time 0 to an adequate time k_2 ($k_1 < k_2$). The equilibrium values in section A are used as the initial values in section B. Thereafter, we extend the section in the same way, and finally, the network operates on the entire time interval corresponding to all sample points. This operation is equivalent to recognizing the shape of the signal by gradually extending the observation section while taking into account the detailed aspects of the signal during its most rapid change.

IV. Simulation Results and Discussion

A) Sample Signals

Sample signals, equivalent to NMR signals that consisted of 1024 data points on a spectrum with a bandwidth of 2000 Hz for the atomic nucleus of phosphorus-31 in a static magnetic field of 2 Tesla, are simulated. The three signals shown in Table 1 and Figs.4-6 were used.

In Table 1, peaks 1 through 7 represent phosphomonoesters (PME), inorganic phosphate (Pi), phosphodiesters (PDE), creatine phosphate (PCr), γ-adenocine triphosphate (γ-ATP), α-ATP, and β-ATP, respectively.

Signal 1 and 3 are equivalent to the spectra of healthy cells with a normal energy metabolism. Pi is relatively small in the spectral components in their signals. Signal 2 is equivalent to the spectrum of a cell that is approaching necrosis. In such cells, the metabolism of energy is decreased and Pi is large in comparison with other components, as shown in Table 1. This signal is analogous to a single-component spectral signal (a monotonic damped signal) compared with signal 1 and 3. Among these signals, only the spectral component A_k is different.

B) Implementation of the network

We next introduce some auxiliary operations that are necessary for stable implementation of the proposed network. The settings of the initial values of the parameters are shown in Table 2. For the amplitude A_k, the amplitudes of the real part and the imaginary part are compared; the larger is divided by 7, the number of signal components; and the result is used as the initial value for all seven components. For the initial values of the frequency f_k and the damping coefficient b_k of each metabolite, rough values are known for f_k and b_k under observation conditions, as described in "NMR spectra" above. Therefore, the initial values were set close to their rough values. All of the initial phases are set to zero.

In the steepest descent method in Eq.(15), two values, 10^{-5} and 10^{-6} are used as ε. By setting the upper limit of the number of the parameter updates to 50,000, we ensure that the units continue to be renewed until the energy function decreases. Then, the parameters can be updated while the energy function is decreasing and the number of renewals does not exceed the upper limit. By using these procedures, it is possible to operate the network in a stable condition. In addition, the following two conditions for stopping the network are set.

(1) The updates of all parameters are terminated.
(2) The energy function reaches an equilibrium point.

The criterion for condition 1 is a limit on the time variation of the parameter P_k: if $dP_k/dt \le 0.01$, we set $dP_k/dt = 0$ and terminate the updating of the parameter.

Regarding condition 2, we judge that the energy function has reached an equilibrium point when the energy function increases, or when the number of updates exceeds the upper limit mentioned above. Theoretically, the network stops and an optimum solution is obtained when the above two conditions are satisfied simultaneously. However, because a monotonic decrease of the energy function is produced by the above-mentioned operations, in practice, we force the network to stop when either of the two conditions occurs.

In each renewal of the unit, we also adjust the network so that the update values do not depart greatly from the actual values by using the prior knowledge of the spectrum outlined in **"Initial values of the parameters"** above. For the frequency f_k, we adopt only values within a range of 0.05 around the values in Table 1. A similar procedure is also carried out for the phase ϕ_k: the range is ±1.0. For the damping coefficient b_k, we adopt only values below 0.1.

As shown in Figs.4-6, the sample signals have decayed to near-zero amplitude after 255 points on the time axis (each full

data set has 1024 points). Therefore, we performed the MSES method for the following three sets of sections:

1. Four sections: [0-63], [0-127], [0-255], [0-1023]
2. Five sections: [0-31], [0-63], [0-127], [0-255], [0-1023]
3. Six sections: [0-15], [0-31], [0-63], [0-127], [0-255], [0-1023]

c) Determination by using modified Hopfield neural network

First parameter estimations of the sample signals are performed using the modified Hopfield neural network without the MSES technique. For signal 1, the result of the determination using $\varepsilon = 10^{-6}$ was better than for $\varepsilon = 10^{-5}$. In the case using $\varepsilon = 10^{-6}$, the spectral composition A_k and the frequency f_k were more accurately estimated than the damping coefficient b_k and the phase ϕ_k. Except for peaks 1 and 2, the errors in A_k were less than 20% in relative terms, and all of the errors in f_k were less than 10%.

Although the effect of the difference in ε became quite small for signals 2 and 3, the same tendency was also shown. However, even using $\varepsilon = 10^{-6}$, the estimation of signals 2 and 3 was not as good as the estimation of signal 1. In these results, all of the errors in f_k are less than 10%, but the only peaks with errors of less than 20% of A_k were peak 3 (about 11%) in signal 2, and peaks 3 (19.7%) and 6 (4.38%) in signal 3.

In summary, the estimation for signal 1 was the best of the three signals. The estimation errors for signals 1 and 2 using $\varepsilon = 10^{-6}$ are shown in Tables 3 and 4.

d) Determination combined with modified sequential extension of section (MSES)

Using the MSES technique, the determination results were improved. For signal 1, which was best estimated using modified Hopfield neural network alone, when we applied the four-section extension method using $\varepsilon = 10^{-6}$, we were able to obtain the best result. For signal 1, the result of the estimation using $\varepsilon = 10^{-6}$ and four sections is shown in Table 5. Compared to Table 3, the accuracy of estimation of the damping coefficient b_k and the phase ϕ_k are improved. However, the accuracy of estimation of the frequency f_k is only slightly improved overall, and the resolution of the spectrum is also only slightly improved. The accuracy of the spectral composition A_k is improved at peaks 2 and 4, but degraded at peaks 1 and 3.

For signal 2, when we applied the MSES technique using six sections with $\varepsilon = 10^{-5}$, the errors were improved overall, compared to using the complex-valued network alone, but we still did not obtain an estimation as accurate as that for signal 1 (Table 6). For signal 3, we could not obtain accurate estimation using any combination of the choices for ε and the number of sections, especially for the spectral composition A_k.

e) Estimation for the signal with noise

Real NMR signals always include noise. Therefore, we need to verify the ability of the proposed method, that is, the modified Hopfield neural network combined with MSES, to estimate parameters for NMR signals that include noise. For that purpose, we used sample signals in which three levels of white Gaussian noise with signal to noise ratios (SNRs) of 10, 5, or 2 were added to signal 1, which was well-estimated compared to other two signals. The SNR is defined as follows:

$$SNR = \sum_{k=0}^{n-1} |F(t_k)|^2 \Big/ n\sigma^2 \qquad (32)$$

Where, $F(t_k)$ is the signal composition at time t_k, σ^2 is the variance of the noise, and n is the total number of sample points (in this case, 1024). The sample signal with SNR = 2 is shown in Fig.8, and the results of the estimation of signals with each SNR are shown in Tables 7-9. For these results, we used $\varepsilon = 10^{-6}$ and the MSES method with four sections.

Comparing these results to those obtained from the sample data with no noise reported in Table 5, there is almost no change in estimation error for the frequency f_k, and the estimation error exceeds 10% only at peak 2 (11.9%) for SNR = 2. For the spectral composition A_k, peaks 4, 5, 6, and 7 had less than 10% error in Table 5. In the case where noise was added with SNR = 2, peaks 4 and 6 are estimated with better than 10% error, but -16.3% is obtained at peak 5 and -21.9% is obtained at peak 7. For the damping coefficient b_k, the peaks with small estimation errors in Table 5 maintain the same error level in the presence of noise. Thus, we conclude that the proposed estimation method is not significantly influenced by noise for the estimation of f_k, A_k, and b_k. However, the phase ϕ_k had greater variation than in Table 5, revealing that the estimation of phase is easily influenced by noise.

f) Discussion

The results of the simulations indicate that the modified Hopfield neural network has the ability to estimate four different parameters of the NMR signal. The simulation results show that the frequency composition f_k and the spectral composition A_k can be estimated with less error than the damping coefficient b_k and the phase ϕ_k. When MSES was applied to this neural network method, it was found that the estimation precisions of b_k and ϕ_k were improved. In addition, it was shown that this combined method experiences no rapid decline in accuracy when applied to signals to which noise was added. However, the optimal sections on which to apply MSES and the optimal step size of ε are different for every simulated NMR signal, and it was verified that they do influence the estimation accuracy.

In the proposed estimation method, preliminary knowledge about the targeted spectrum is indispensable when determining the initial value of the parameters and updating them during the estimation process. If there is no preliminary knowledge, the network must search for the solution in an unlimited solution space, and the probability of reaching an optimum solution in a reasonable time period becomes very small. In addition, because the steepest-descent method is used to update the parameters, it is difficult for the network to reach the optimum solution if it starts from inappropriate initial values.

MSES uses the equilibrium values of the parameters calculated using one section as the initial values for the following section in a sequence. In other words, every time a section is extended, the neural network is used to minimize a new energy function with new initial values and a new group of data. Therefore, when calculation on the new section begins, the direction in which a minimum solution has previously been sought is reset, and the network is free to search in another direction. This may reduce the danger of falling into a local minimum solution. However, when the damping of the target signal is monotonic (depending on the determination of the initial section), it appears that the search direction may no longer be effectively reset and the network cannot escape from a local solution.

The signal in Fig.7, which contains noise, maintains the characteristics of the initial damping for the noise-free version of the same signal in Fig.4. It seems that this fact was advantageous in MSES. Therefore, comparably stable estimation accuracy in the presence of noise is obtained using preliminary knowledge of the parameters and the MSES method.

Usually, a Hopfield network cannot reach the optimum solution from a local solution without restarting from different initial values [6]. MSES carries out this operation automatically. A Boltzmann machine [5,11,16] might be used to avoid local solutions and approach the optimum solution. However, in that method, the state of the network is not indeterminate and it is changed stochastically. Thus, stability of the decrease in energy with state transitions is not guaranteed. Compared with the avoidance of the local solution by the Boltzmann machine, MSES seems to be more elegant because it is free of the uncertainty associated with the stochastic operation. However, the stability of convergence to the optimal solution is influenced by the damping state of the targeted signal, and we must overcome this problem.

V. Conclusion

An efficient modified Hopfield neural network for NMR spectrum estimation has been presented. The main valuable achievement of this paper is that the estimation operation is accelerated by performing cross correlation in the frequency domain between the input data and the input weights of neural networks. Unlike the conventional quantitative methods of NMR spectrum estimation using hierarchical neural networks, the proposed algorithm does not need a learning process. In addition, the MSES method has been devised and used in combination with Hopfield neural network in order to take into account the damping state of the NMR signal. For performance evaluation of the proposed estimation method, simulations have been carried out using sample signals composed of seven different metabolites to simulate in vivo ^{31}P-NMR spectra, with and without added noise.

Simulations results have shown that the proposed method has the ability to estimate the modeling parameters of the NMR signal. However, it was also shown that its ability differs according to the damping state of the signals.

The investigation here has indicated that MSES reduces the danger of falling into a local minimum in the search for the optimum solution using a Hopfield neural network. Although there another technique such as a Boltzmann machine might be used to avoid local solutions, it is stochastic and requires much futile searching before it reaches the optimum solution. On the other hand, it has been observed that the proposed method could find the optimum solution stably if the variation in the targeted signal could be identified accurately.

References

[1] Ala-Korpela, M., Changani, K.K., Hiltunen, Y., Bell, J.D., Fuller, B.J., Bryant, D.J., Taylor-Robinson, S.D. and Davidson, B.R. , "Assessment of quantitative artificial neural network analysis in a metabolically dynamic ex vivo 31P NMR pig liver study," *Magnetic Resonace in Medicine*, vol. 38, 1997, pp. 840-844.

[2] Belliveau, J.W., Kennedy Jr, D.N., McKinstry, R.C., Buchbinder, B.R., Weisskoff, R.M., Cohen, M.S., Vevea, J.M., Brandy, T.J. and Rosen, B.R., "Functional mapping of the human visual cortex by magnetic resonance imaging," *Science*, vol. 254, no.5032, 1991, pp.716-719.

[3] Benvenuto, N. and Piazza, F., "On the complex backpropagation algorithm. *Institute of Electrical and Electronic Engineers,"* IEEE Transaction on Signal Processing, vol. 40, no. 4, 1992., pp. 967-969.

[4] Cooley, J.W. and Tukey, J.W. "An algorithm for machine calculation of complex Fourier series," *Mathematics and Computation,* vol. 19 , no. 90, 1965, pp. 297-301.

[5] David, H.A., Hinton, G.E. and Sejnowski, T.J., "A Learning Algorithm for Boltzmann Machines," Cognitive Science: *A Multidisciplinary Journa*l, vol. 9, no. 1, 1985, pp. 149-169.

[6] Dayhoff, J.E., *Neural Network Architectures*: *An Introduction*. New York, USA: Van Nostrand Reinhold, 1989.

[7] Derome, A.E.. *Modern NMR Techniques for Chemistry Research* (*Organic Chemistry Series, Vol 6*), Oxford, United Kingdom: Pergamon Press, 1987.

[8] El-Bakry, H..M., "New Fast Time Delay Neural Networks Using Cross Correlation Performed in the Frequency Domain," *Neurocomputing Journal*, vol. 69, 2006, pp. 2360-2363.

[9] El-Bakry, H.M. and Zhao, Q., "Fast Time Delay Neural Networks," *International Journal of Neural Systems*, vol. 15, no. 6, 2005, pp. 445-455.

[10] Feinberg, D.A. and Oshio, K., "GRASE (gradient and spin echo) MR imaging: A new fast clinical imaging technique," *Radiology*, vol. 181, pp. 597-602.

[11] Geman, S. and Geman, D., "Stochastic Relaxation, Gibbs Distribution and the Bayesian Restoration of Images," *IEEE Transactions on Pattern Analysis and Machine Intelligence*, vol. 6, 1984, pp. 721-741.

[12] Georgiou, G. M. and Koutsougeras, C. , "Complex domain backpropagation," *IEEE Transactions on Circuits and System*," *Analog and Digital Signal Processing*, vol. 39 no. 5, 1992, pp. 330-334.

[13] Han, L. and Biswas, S.K., "Neural networks for sinusoidal frequency estimation," *Journal of The Franklin Institute*, vol. 334B, no. 1, 1997, pp. 1-18.

[14] Haselgrove, J.C., Subramanian, V.H., Christen, R. and Leigh, J.S., "Analysis of in-vivo NMR spectra," *Reviews of Magnetic Resonance in Medicine*, vol. 2, 1988, pp. 167-222.

[15] Henning, J., Nauerth, A. and Fnedburg, H., "RARE imaging: A first imaging method for clinical MR," *Magnetic Resonance in Medicine*, vol. 3, no. 6, 1986, pp. 823-833.

[16] Hinton, G.E. and Sejnowski, T.J., "*Learning and Relearning in Boltzmann Machine," Parallel distributed processing: explorations in*

the microstructure of cognition, vol. 1: foundations (pp. 282-317). Cambridge, MA, USA: MIT press, 1986.

[17] Hirose, A., "Dynamics of fully complex-valued neural networks," *Electrronics Letters*, vol. 28, no. 16, 1992a, pp. 1492-1494.

[18] Hirose, A., "Proposal of fully complex-valued neural networks," *Proceedings of International Joint Conference on Neural Networks*: *Vol. 4*, 1992b, pp. 152-157, Baltimore, MD, USA.

[19] Hopfield, J.J., "Neural networks and physical systems with emergent collective computational abilities," *Proceeding of National Academic of Science in USA: Vol. 79*, 1982, pp. 2554-2558.

[20] Hopfield, J.J., "Neurons with graded response have collective computational properties like those of two-state neurons," *Proceeding of National Academic of Science in USA, Vol. 81*, 1984, pp. 3088-3092.

[21] Jankowski, S., Lozowski, A. and Zurada, J.M., "Complex-valued multistate neural associative memory," *Proceedings of IEEE Transactions on Neural Networks*, vol. 7, no. 6, 1996, pp. 1491-1496.

[22] Kaartinen, J., Mierisova, S., Oja, J.M.E., Usenius, J.P., Kauppinen, R.A. and Hiltunen, Y., "Automated quantification of human brain metabolites by artificial neural network analysis from in vivo single-voxel 1H NMR spectra," *Journal of Magnetic Resonance*, vol. 134, 1998, pp. 176-179.

[23] Kuroe, Y., Hashimoto. N. and Mori, T., " On energy function for complex-valued neural networks and its applications," Neural information proceeding, *Proceedings of the 9th International Conference on Neural Information Processing. Computational Intelligence for the E-Age. Vol.3*, 2002, pp. 1079-1083.

[24] Kwong, K., Belliveau, J.W., Chesler, D.A., Goldberg, I.E., Weisskoff, R.M., Poncelet, B.P., Kennedy, D.N., Hoppel, B.E., Cohen, M.S., Turner, R., Cheng, H., Brady, T.J. and Rosen, B.R., "Dynamic magnetic resonance imaging of human brain activity during primary sensory stimulation," *Proceedings of the National Academy of Sciences, vol 89, no. 12, 1992, pp. 5675-5679.*

[25] Maddams, W.F., "The scope and Limitations of Curve Fitting," *Applied Spectroscopy, vol. 34, no. 3, 1980, pp. 245-267.*

[26] Mansfield, P., "Multi-planar image formation using NMR spin echoes," *Journal of Physical C: Solid State Physics*, vol. 10, 1977, pp. 55-58.

[27] Melki, P.S., Mulkern, R.V., Panych, L.S. and Jolesz, F.A. , "Comparing the FAISE method with conventional dual-echo sequences," *Journal of Magnetic Resonance Imaging*, vol. 1, 1991, pp. 319-326.

[28] Meyer, C.H., Hu, B.S., Nishimura, D.G. and Macovski, A. , "Fast Spiral Coronary Artery Imaging," *Magnetic Resonance in Medicine*, vol. 28, no. 2, 1992, pp. 202-213.

[29] Miersová, S. and Ala-Korpela, M., "MR spectroscopy quantification: a review of frequency domain methods," *NMR in Biomedicine*, vol.14, 2001, pp.247-259.

[30] Morita, N. and Konishi, O., "A Method of Estimation of Magnetic Resonance Spectroscopy Using Complex-Valued Neural Networks," *Systems and Computers in Japan*, vol. 35, no. 10, 2004, pp. 14-22.

[31] Naressi, A., Couturier, C., Castang, I., de. Beer, R. and Graveron-Demilly, D., "Java-based graphical user interface for MRUI, a software package for quantitation of in vivo medical magnetic resonance spectroscopy signals," *Computers in Biology and Medicine*, vol.31, 2001, pp. 269-286.

[32] Nitta, T., "An Extension of the Back-Propagation Algorithm to Complex Numbers," *Neural Networks*, vol. 10, no. 8, 1997, pp. 1392-1415.

[33] Nitta, T., "An Analysis of the Fundamental Structure of Complex-Valued Neurons," *Neural Processing Letters*, vol. 12, no. 3, 2000, pp. 239-246.

[34] Nitta, T., "Redundancy of the Parameters of the Complex-valued Neural Networks. *Neurocomputing*," vol. 49, no. (1-4), 2002, pp. 423-428.

[35] Nitta, T., "On the Inherent Property of the Decision Boundary in Complex-valued Neural Networks," *Neurocomputing*, vol. 50(c), 2003, pp. 291-303.

[36] Nitta, T., "Solving the XOR Problem and the Detection of Symmetry Using a Single Complex-valued Neuron," *Neural Networks*, vol. 16, no. 8, 2003, pp. 1101-1105.

[37] Nitta, T., "The Uniqueness Theorem for Complex-valued Neural Networks and the Redundancy of the Parameters," *Systems and Computers in Japan*, vol. 34, no.14, 2003, pp. 54-62.

[38] Nitta, T., " Orthogonality of Decision Boundaries in Complex-Valued Neural Networks," *Neural Computation*, vol. 16, no.1, 2003, pp73-97.

[39] Nitta, T., " Reducibility of the Complex-valued Neural Network," *Neural Information Processing - Letters and Reviews*, vol. 2, no. 3, 2004, pp. 53-56.

[40] Ogawa, S., Lee, T.M., Nayak, A.S. and Glynn, P., "Oxygenation-sensitive contrast in magnetic resonance image of rodent brain at high magnetic fields," *Magnetic Resonance in Medicine*, vol. 14, no. 1, 1990, pp. 68-78.

[41] Provencher, S., W., " Automatic quantification of localized in vivo ^{1}H spectra with LCModel," *NMR in Biomedicine*, vol. 14 no. 4, 2001, pp. 260-264.

[42] Rumelhart, D,E, Hinton, G.E. and Williams, R.J., *Learning internal representations by error propagation, In Rumelhart, D,E and McClelland, J.L.(Eds.), Parallel Distributed Processing: Volume 1:Foundations* (pp.318-362), Cambridge, MA, USA: MIT press, 1986.

[43] van den Boogaart, A., Van Hecke, P., Van Hulfel, S., Graveron-Dermilly, D., van Ormondt, D. and de Beer, R., "MRUI: a graphical user interface for accurate routine MRS data analysis," *Proceeding of the European Society for Magnetic Resonance in Medicine and Biology 13th Annual Meeting*, Prague, (p.318), 1996.

[44] van Huffel, S., Chen, H., Decanniere, C. and Hecke, P.V. , "Algorithm for time-domain NMR data fitting based on total least squares.," *Journal of Magnetic Resonance A*, vol. 110, pp. 228-237.

[45] Sijens, P.E., Dagnelie, P.C., Halfwrk, S., van Dijk, P., Wicklow, K. and Oudkerk, M., "Understanding the discrepancies between 31P MR spectroscopy assessed liver metabolite concentrations from different institutions," *Magnetic Resonance Imaging*, vol. 16, no. 2, 1998, pp. 205-211.

[46] Zhou, C. and Liu, L., "Complex Hopfield model," *Optics Communications*, vol. 103, no. 1-2, 1993, pp. 29-32.

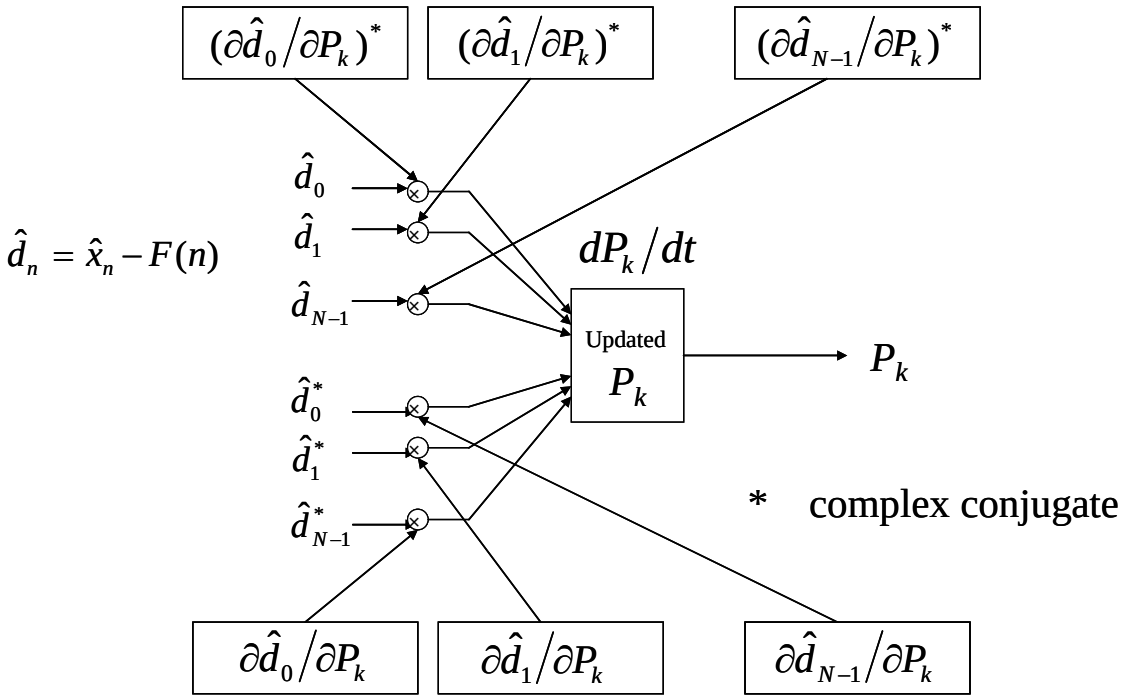

Fig.1 Structure of the modified Hopfield neural network

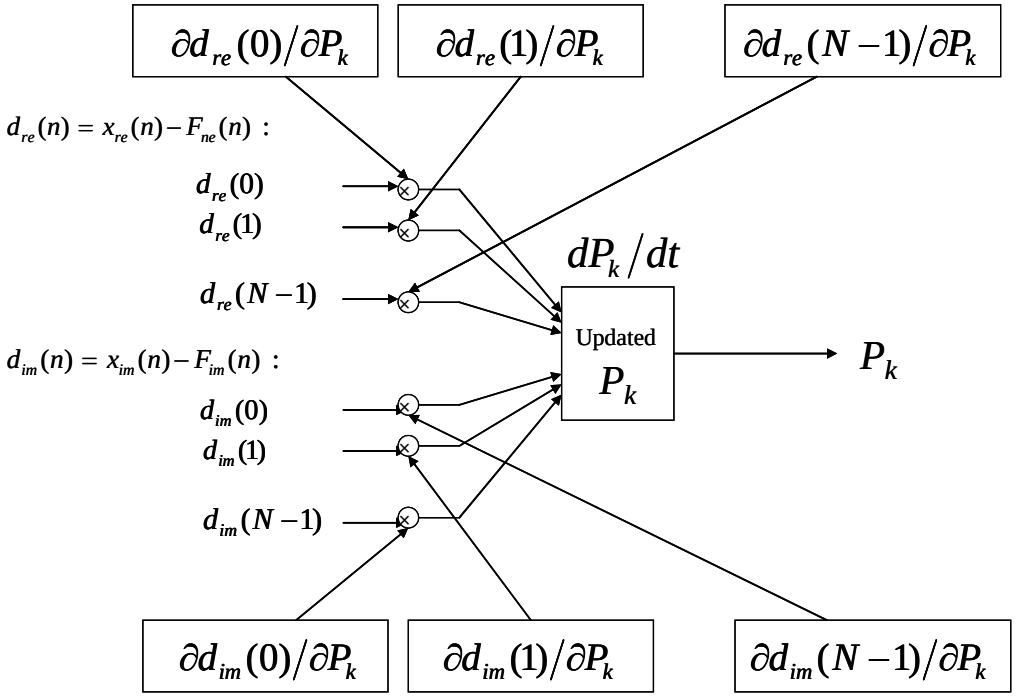

Fig.2 The structure of real-valued network equivalent to complex-valued network of Fig.1

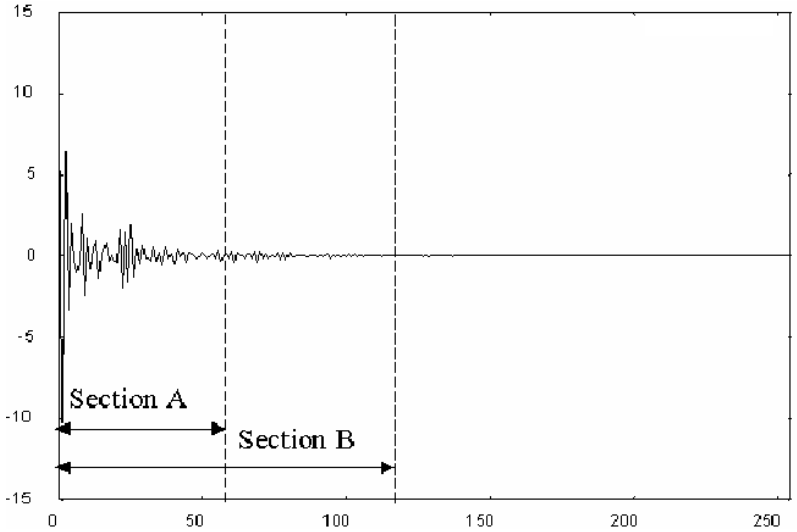

Fig.3 Illustration of the modified sequential extension of section (SES) method.

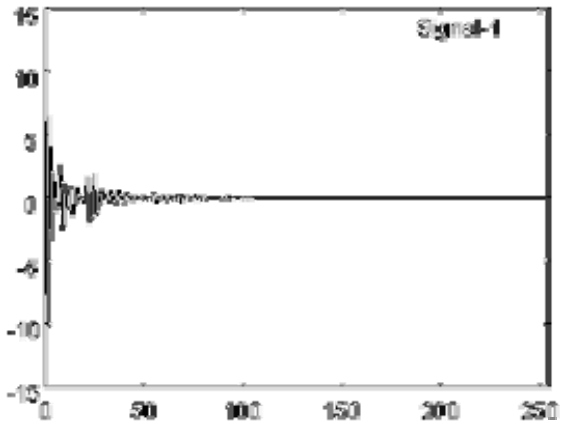

Fig.4 Signal 1

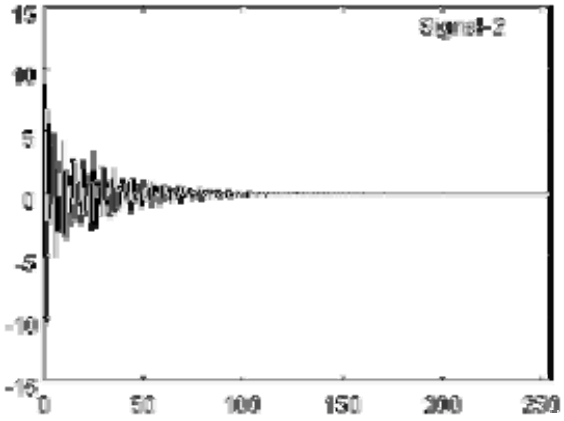

Fig.5 Signal 2

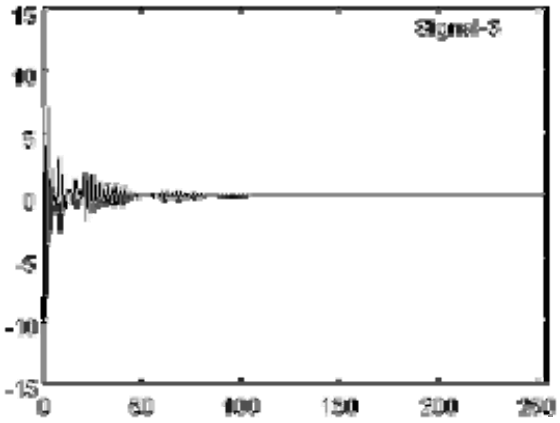

Fig.6 Signal 3

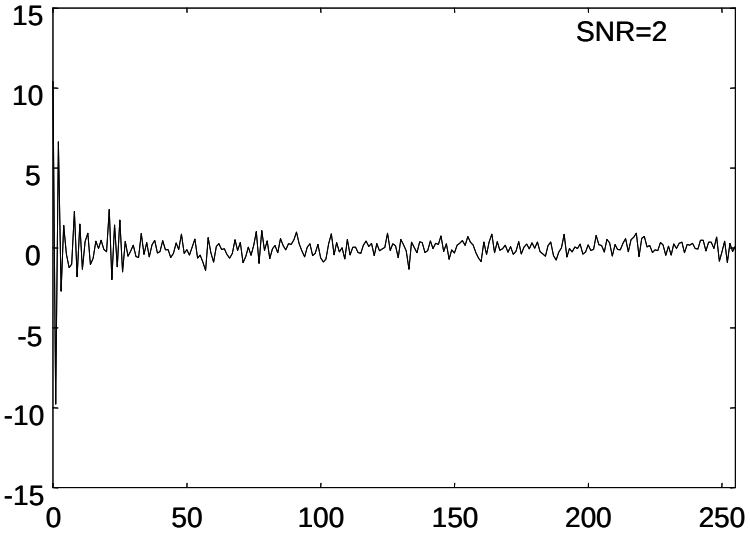

Fig.7 Noisy NMR signal with SNR = 2.

TABLE I. PARAMETERS OF SAMPLE SIGNALS

Peak	f_k*	b_k	Φ_k**	A_k (1)	A_k (2)	A_k (3)
1	0.368	0.05395	0.4774	0.726	0.7	0.996
2	0.397	0.03379	0.3699	1.02	6.246	0.5
3	0.435	0.05918	0.2296	2.1	1.8	2.1
4	0.485	0.03785	0.051	2.37	1.2	3.6
5	0.526	0.04858	-0.1002	1.89	0.5	1.15
6	0.616	0.05744	-0.4264	2.04	0.5	2.2
7	0.763	0.04035	-0.9657	1.1	0.3	0.7

TABLE II. INITIAL VALUES OF PARAMETERS

Peak	f_k	b_k	Φ_k	A_k (1)	A_k (2)	A_k (3)
1	0.35	0.1	0.0	1.481595	1.502836	1.505209
2	0.4	0.1	0.0	1.481595	1.502836	1.505209
3	0.45	0.1	0.0	1.481595	1.502836	1.505209
4	0.5	0.1	0.0	1.481595	1.502836	1.505209
5	0.55	0.1	0.0	1.481595	1.502836	1.505209
6	0.6	0.1	0.0	1.481595	1.502836	1.505209
7	0.75	0.1	0.0	1.481595	1.502836	1.505209

TABLE III. THE ESTIMATED ERROR (%) OF SIGNAL 1 USING THE COMPLEX-VALUED NEURAL NETWORK

Peak	f_k	b_k	Φ_k	A_k
1	7.82	-20.9	-83.4	58.9
2	9.65	195.9	-25.4	37.5
3	0.16	57.5	22.9	-14.6
4	0.47	-32.9	-100.4	-19.9
5	0.08	-29.3	-13.1	-2.1
6	-0.28	-2.92	49.3	-3.97
7	0.05	0.77	0.58	0.45

TABLE IV. THE ESTIMATED ERROR (%) OF SIGNAL 2 USING THE COMPLEX-VALUED NEURAL NETWORK

Peak	f_k	b_k	Φ_k	A_k
1	7.80	-61.4	-109.5	258.4
2	0.29	3.0	47.0	-66.7
3	-8.05	-53.2	-421.0	11.1
4	-0.78	164.2	-625.1	38.0
5	-4.94	105.8	180.5	206.4
6	-0.75	74.0	-55.9	97.4
7	-1.68	147.8	-111.1	98.2

TABLE V. THE ESTIMATED ERROR (%) OF SIGNAL 1 WITH MODIFIED SEQUENTIAL EXTENSION OF SECTION USING 4 SECTIONS ($E = 10^{-6}$)

Peak	f_k	b_k	Φ_k	A_k
1	8.67	-20.8	-163.2	78.9
2	5.26	195.9	6.84	28.4
3	-0.11	-15.1	123.4	-18.8
4	0.04	-3.9	55.9	-4.3
5	0.08	-0.5	3.4	-1.2
6	0.02	-1.83	-2.1	-1.96
7	0.09	-2.03	-0.99	-2.1

TABLE VI. THE ESTIMATED ERROR (%) OF SIGNAL 2 WITH MODIFIED SEQUENTIAL EXTENSION OF SECTION USING 6 SECTIONS ($E = 10^{-5}$)

Peak	f_k	b_k	Φ_k	A_k
1	-0.33	85.4	-220.8	205.7
2	-2.14	96.2	170.3	29.1
3	3.59	68.8	-535.5	26.7
4	0.39	43.7	55.2	38.2
5	0.87	39.9	365.1	50.2
6	-0.10	15.7	-21.3	19.3
7	-0.30	5.84	-45.5	2.40

TABLE VII. THE ESTIMATED ERROR (%) OF SIGNAL 1 WITH NOISE, SNR = 10

Peak	f_k	b_k	Φ_k	A_k
1	8.69	-13.7	-135.6	91.7
2	6.78	195.9	-0.53	15.3
3	0.14	-26.7	82.7	-31.4
4	-0.04	2.01	144.7	0.97
5	0.13	-1.59	-24.1	0.26
6	0.03	4.14	4.92	-0.34
7	0.16	-4.83	-3.54	-5.45

TABLE VIII. THE ESTIMATED ERROR (%) OF SIGNAL 1 WITH NOISE, SNR = 5

Peak	f_k	b_k	Φ_k	A_k
1	8.67	-31.5	-111.1	81.8
2	7.68	195.9	-16.40	15.9
3	0.16	-31.2	49.2	-34.6
4	0.04	-11.0	38.2	-8.31
5	0.27	-1.34	-115.5	0.11
6	-0.16	1.83	18.6	4.75
7	0.08	11.4	-3.55	5.0

TABLE IX. THE ESTIMATED ERROR (%) OF SIGNAL 1 WITH NOISE, SNR = 2

Peak	f_k	b_k	Φ_k	A_k
1	8.39	-60.4	-121.8	26.7
2	11.9	195.9	-60.4	72.6
3	0.29	-18.9	-216.4	-24.8
4	-0.29	9.33	420.4	7.97
5	0.17	-22.2	-53.7	-16.30
6	-0.52	-1.49	49.4	-5.54
7	0.07	-3.84	-1.44	-21.9